Experimental ultrasound characterization of red blood cell aggregation using the structure factor size estimator

François T. H. Yu[a] and Guy Cloutier[b]
Laboratory of Biorheology and Medical Ultrasonics, University of Montreal Hospital Research Center, Pavilion J.A. de Sève (Room Y-1619), 2099 Alexandre de Sève, Montréal, Québec, H2L 2W5, Canada

(Received 3 October 2006; revised 5 April 2007; accepted 6 April 2007)

The frequency dependence of the ultrasonic backscattering coefficient (BSC) was studied to assess the level of red blood cell (RBC) aggregation. Three monoelement focused wideband transducers were used to insonify porcine blood sheared in a Couette flow from 9 to 30 MHz. A high shear rate was first applied to promote disaggregation. Different residual shear rates were then used to promote formation of RBC aggregates. The structure factor size estimator (SFSE), a second-order data reduction model based on the structure factor, was applied to the frequency-dependent BSC. Two parameters were extracted from the model to describe the level of aggregation at 6% and 40% hematocrits: *W*, the packing factor, and *D* the aggregate diameter, expressed in number of RBCs. Both parameters closely matched theoretical values for nonaggregated RBCs. *W* and *D* increased during aggregation with stabilized values modulated by the applied residual shear rate. Furthermore, parameter *D* during the kinetics of aggregation at 6% hematocrit under static conditions correlated with an optical RBC aggregate size estimation from microscopic images ($r^2=0.76$). To conclude, the SFSE presents an interesting framework for tissue characterization of partially correlated dense tissues such as aggregated RBCs. © *2007 Acoustical Society of America.*
[DOI: 10.1121/1.2735805]

PACS number(s): 43.80.Qf, 43.80.Cs, 43.35.Yb [FD] Pages: 645–656

I. INTRODUCTION

Ultrasonic tissue characterization (UTC) is emerging as a unique noninvasive tool to characterize red blood cell (RBC) aggregation in vivo. UTC is an imaging modality that takes advantage of quantitative ultrasonic parameters (backscattering, attenuation, speed of sound, tissue nonlinearity, statistics) to reveal intrinsic tissue properties. Major advances in this field have been recently accomplished in the areas of prostate cancer diagnosis,[1] cell apoptosis monitoring,[2,3] osteoporosis characterization,[4] rat fibroadenomas and mouse mammary carcinomas characterization,[5,6] and in early Duchenne muscular dystrophy diagnosis.[7] In most cases, the spectral content (integrated backscatter coefficient, spectral slope, *y* intercept, midband fit) of the rf ultrasound signal backscattered by the tissue is used to extract its acoustic properties and to reveal its microstructure and composition.

In the ultrasonic blood characterization (UBC) field, the objective is to obtain quantitative parameters that reflect the aggregation state of blood elements. It is well known that RBCs aggregate to form complex three-dimensional (3D) rouleaux structures depending mainly on an equilibrium between aggregating forces, which are mediated by RBC membrane factors and concentrations of plasmatic high molecular weight proteins such as fibrinogen, and disaggregating forces induced by the shear effects of the flow and the electrostatic and steric interactions between RBCs.[8] This phenomenon is normal, reversible, and it occurs in the circulation of many mammalian species. RBC hyper-aggregation, however, is a pathological state; clinical and epidemiological studies identified it as an independent risk factor of circulatory related disorders such as deep venous thrombosis,[9] atherosclerosis,[10] and diabetes mellitus,[11] to name a few. Because these diseases are characterized by localized blood and blood vessel impairments, this suggests that flow-dependent rheological parameters, such as RBC aggregation, could be involved in their respective pathogenesis. It would thus be of great interest to elucidate the role of RBC aggregation in the etiology of these pathologies *in vivo* and *in situ* with UBC techniques.

One difficulty in UBC resides in the fact that blood is an extremely dense medium (5 million erythrocytes/mm^3) that introduces a nonlinear relationship between the backscattered power and the scatterer concentration. In fact, nonlinear effects become important above 10% hematocrit (*H*, which is the RBC volume concentration), approximately.[12] The physiological hematocrits normally range from 35% to 45%, which is clearly in the nonlinear regime. This particularity is a major difficulty in blood acoustic characterization compared to the other UTC fields, where the number density of scatterers in the targeted tissues rarely exceeds 100 scatterers/mm^3.[13,14] Another major challenge of UBC is to consider clustering particles as RBC aggregates.

The nonlinear hematocrit dependence of the BSC has been thoroughly studied with nonaggregating RBC suspensions. It is well described for Rayleigh scatterers at frequencies up to 90 MHz by the Perkus Yevick packing factor W_{PY},[15,16] and it is supported by quantitative experimental data.[12,17] In the frequency domain, the spectrum of nonaggregating RBCs presents a spectral slope (SS) of 4 (SS is the linear slope of the backscatter as a function of frequency on

[a]Electronic mail: francois.yu@polymtl.ca
[b]Electronic mail: guy.cloutier@umontreal.ca

a log-log scale). When considering aggregating RBCs, an increase in the effective scatterer size (caused by RBC rouleaux formation) or in the insonifying ultrasound (US) frequency (to achieve better resolution) both increase the ka product and restrain the validity of the Rayleigh scattering theory (k is the ultrasonic wave number, and a is the mean radius of individual scatterers or RBCs). Nevertheless, numerous experimental quantification of the effect of RBC aggregation on the backscattering coefficient (BSC) and its frequency dependence can be found in the literature.[18–24] Previously, our group reported different simulation models based on the structure factor, $S(-2k)$, that could explain the frequency dependence of aggregating RBCs in the non-Rayleigh regime.[25–28] It is the purpose here to validate those models with experimental results. The objective of the present study was thus to use an inverse approach of data reduction, using the structure factor size estimator (SFSE), to analyze experimental results obtained from three different wideband focused transducers covering the bandwidth from 9 to 30 MHz. Two parameters that describe the structure of aggregated RBCs were extracted from the second-order Taylor expansion of the structure factor. The first parameter W translates acoustically into variations of the BSC, whereas D reflects reductions of SS from its Rayleigh value of 4.

The theoretical framework behind modeling of the structure factor is first described in Sec. II. Section III explains the experimental setup followed by Sec. IV that gives results on the kinetics of 6% and 40% hematocrit aggregating RBCs, sheared in a Couette flow at residual shear (RS) rates of 0, 2, 10, and 30 s^{-1}. For the static residual shear rate (RS0) at 6% hematocrit, results are compared to aggregate sizes estimated by optical microscopic image segmentation. The validation of the method is discussed in Sec. V.

II. THEORY: THE STRUCTURE FACTOR SIZE ESTIMATOR

Suspended RBCs in a saline solution (no aggregation) can be acoustically considered as a dense collection of partially correlated weak scatterers embedded in a homogeneous medium.[29] Using the Born approximation, the backscattered power is given for Rayleigh scatterers ($ka \ll 1$) by[12]

$$\mathrm{BSC}(-2k) = m\sigma_b(-2k)W, \tag{1}$$

where m is the number density of scatterers, σ_b is the backscattering cross section of a single RBC, W is the packing factor, and k is the wave vector. For suspended RBCs in saline, all parameters in Eq. (1) can be determined analytically. When the hematocrit is known by microcentrifugation, m is given by $m=H/V_s$, where V_s is the volume of a RBC (typically 87 μm^3). The backscattering cross-section σ_b of a Rayleigh scatterer can be estimated by[14]

$$\sigma_b(-2k) = \frac{1}{4\pi^2} V_s^2 \gamma_Z^2 k^4 \left(3\frac{\sin(2ka) - 2ka\cos(2ka)}{(2ka)^3} \right)^2, \tag{2}$$

where γ_Z is the acoustical relative impedance mismatch between the RBC and its suspending medium, hence $\gamma_Z = (Z_{\mathrm{RBC}} - Z_{\mathrm{plasma}})/Z_{\mathrm{plasma}}$ (see Table I). The packing factor W has been extensively studied for nonaggregating scatterers.[30,31] It was shown to reflect the decrease in backscattered power with the increase in spatial correlation among particles with increasing particle crowding. W can be seen as a correction factor that accounts for increasing destructive phase interference (coherent field) introduced by the increase in correlation between particles. The detailed development of this approach can be found in Twersky's paper.[30] In the same manuscript, expressions of the Perkus–Yevick packing factor W_{PY} (hard particles) were proposed for packed spheres ($W_{\mathrm{PY}s}$) and cylinders ($W_{\mathrm{PY}c}$). They are functions of the hematocrit H,

TABLE I. Some physical properties of blood (Ref. 48). The density is denoted ρ, the adiabatic compressibility κ, and the acoustic impedance Z.

	ρ (kg m^{-3})	κ (Pa^{-1})	Z (kg m^{-2} s^{-1})
RBC	1078	3.50×10^{-10}	1.755×10^{6}
Plasma	1021	4.09×10^{-10}	1.580×10^{6}
Relative impedance contrast γ_Z	⋯	⋯	0.11

$$W_{\mathrm{PY}s}(H) = \frac{(1-H)^4}{(1+2H)^2}, \tag{3}$$

$$W_{\mathrm{PY}c}(H) = \frac{(1-H)^3}{(1+H)}. \tag{4}$$

The cylinder prototype [Eq. (4)] provided the best fitting with experimental measurements for suspended RBCs up to physiological hematocrits under Rayleigh conditions.[12] However, this Rayleigh theoretical approach cannot be used when aggregating RBCs are considered and non-Rayleigh scattering occurs. Looking at Eq. (1), one can consider different ways to model the power increase with RBC aggregation. The effect of aggregation can be considered by an increase in the effective scatterer cross section (rouleaux formation) combined to a decrease in the number of scatterers at a constant hematocrit.[32] A comprehensive study of the effect of aggregation on W should then be pursued, as it would not be a simple function of H. A different approach[25–28] introduced the structure factor $S(-2k)$ as an alternative way to model the backscatter power in the non-Rayleigh regime. These last models were based upon the generalized form of Eq. (1), also introduced in Ref. 30, namely:

$$\mathrm{BSC}(-2k) = m\sigma_b(-2k)S(-2k). \tag{5}$$

With this formalism, the number density of scatterers m and the backscattering cross section of a single red cell σ_b remain constant, and changes in backscattered power are entirely caused by variations of the structure factor $S(-2k)$, which is by definition the Fourier transform of the pair correlation function $g(r)$:[30]

$$S(-2k) = 1 + m\int (g(r)-1)e^{-j2kr}dr. \tag{6}$$

In this expression, $g(r)$ represents the probability of finding two particles separated by a distance r (see Figs 9 and 10 of Ref. 26 for a visual interpretation of this parameter). This formula shows that a variation in the microscopic organiza-

tion of particles, and thus of $g(r)$, modifies $S(-2k)$ and therefore also the BSC. It is proper to emphasize here that the low frequency limit of $S(-2k)$ is by definition[30] the packing factor W:

$$S(-2k)|_{k\to 0} = 1 + m\int (g(r)-1)dr = W. \quad (7)$$

Under Rayleigh conditions (nonaggregated RBCs), Eq. (5) therefore directly reduces to Eq. (1).

A second-order Taylor approximation of $S(-2k)$ is proposed here to extract two geometrical parameters from the rf frequency-dependent backscattered US data. The second-order Taylor expansion in k of $S(-2k)$ is of the form:

$$S(-2k) \approx C_0 + (-2k)C_1 + (-2k)^2 C_2, \quad (8)$$

where C_0, C_1, and C_2 are simply the series coefficients. We have shown earlier that $C_0 = S(-2k)|_{k=0}$ is the packing factor W. The second constant C_1 is necessarily equal to zero because of parity (i.e., if the blood sample is turned around 180°, the tissue remains the same). Since $S(-2k)$ is a nondimensional number, the third constant C_2 must be a surface in m^2. This inference is well known in crystallography, using small angle neutron, light, and x-ray scattering to determine polymer and protein radius of gyration. C_2 is negative and $-C_2$ is related to the square of the radius of gyration (R_g) of scatterers. This second-order approximation is valid in the Guinier region,[33] named after the pioneering work of that scientist in x-ray scattering and is discussed in Sec. V. In the current paper, we consider that $C_2 = -R_g^2$, hence

$$S(-2k) \approx W - 4R_g^2 k^2. \quad (9)$$

For identical spherical scatterers of radius a (i.e., individual RBCs), and recombining Eqs.(2), (5), and (9), we find that

$$\mathrm{BSC}(-2k) = \frac{1}{3\pi} H \gamma_Z^2 k^4 a^3 \left(3\frac{\sin(2ka) - 2ka\cos(2ka)}{(2ka)^3}\right)^2 \times (W - 4R_g^2 k^2). \quad (10)$$

By replacing $k = 2\pi f/c$, Eq. (10) becomes a polynomial approximation of the frequency dependence of the backscatter for aggregating RBCs, which can model the decrease in spectral slope observed experimentally in the non-Rayleigh regime. By considering an isotropic 3D aggregate of radius R, R_g is related to R by $R_g = \sqrt{\frac{3}{5}}R$.[33] Hence, $D = \sqrt{\frac{5}{3}}R_g/a$, where D is the isotropic diameter of an aggregate (expressed in number of RBCs).

In the current study, the SFSE was used to achieve data reduction of experimental BSC measurements on aggregating RBCs. Estimated values of W and D were deduced from Eq. (10) by least mean squared polynomial fitting of the BSC as a function of frequency.

III. MATERIALS AND METHODS

A. Blood preparation

Fresh porcine whole blood was obtained from a local slaughter house. It was anti-coagulated with 3 g/L of ethylene diamine tetra acetic acid (EDTA). The buffy coat was removed after centrifugation at 2000g and four 60 mL samples were prepared as described in Table II. These samples were introduced and sheared in a Couette flow system, as in Refs. 23 and 24, where US measurements were performed. All experiments were made at room temperature.

TABLE II. Labeling of the different types of blood samples studied.

Label	Hematocrit (%)	Suspending medium
H6	6	Isotonic saline
T6	6	Porcine plasma
H40	40	Isotonic saline
T40	40	Porcine plasma

B. US setup and normalization algorithm for BSC

The use of focused transducers allows one to overcome the limited signal to noise ratio consequent to increased attenuation in high frequency characterization of blood (>20 MHz), especially at physiological hematocrits. However, it was shown that with a focused transducer, the standard substitution method can yield erroneous BSC results.[34] One normalization technique with focused transducers was suggested using a low density 6% hematocrit RBC suspension, with the condition that the BSC of the reference suspension is known or can be determined.[15] Accordingly, the methodology that follows was utilized to first determine the 6% hematocrit reference $\mathrm{BSC}_{\mathrm{H6}}$, which was then used for assessing the backscattering coefficients of blood with the Couette flow apparatus.

Three broadband transducers were used in these experiments. Their general characteristics are summarized in Table III. The pulse-echo acquisition system was composed of an Avtech pulse generator (model AVB2-TA-C-CRIMA, Ottawa, Canada), a Ritec diplexer (model RDX-6, Warwick, RI), a 10 dB Mitec linear amplifier (model AU-A3-0120, Hauppauge, NY), a Panametric pulser-receiver that was used as a wideband receiver (model 5900 PR, Waltham, MA), and an 8 bit 500 MHz sampling frequency GageScope acquisition board (model 8500CS, Montreal, Canada). The first step consisted in determining the $\mathrm{BSC}_{\mathrm{H6}}$. The H6 sample was stirred in a beaker with a magnetic agitator to avoid sedimentation. One-hundred rf lines were acquired and stored; the procedure was repeated on a stainless steel plane reflector

TABLE III. Characteristics of each transducer used to collect rf US data.

Type (manufacturer)	Center frequency (MHz)	−3 dB bandwidth (MHz)	Transducer radius (mm)	Focal length (mm)
V313-SM (Panametrics, Waltham, MA)	15	9–14[a]	4.5	12
V317-SM (Panametrics)	20	15–26	4.5	12
PVDF (VisualSonics, Toronto, Canada)	35	26–40[b]	1.5	6

[a]The 15 MHz transducer was excited at a lower frequency to cover a different frequency band than the 20 MHz transducer.
[b]For the 35 MHz transducer, according to the Guinier plot of Fig. 11, only the data under 30 MHz were used.

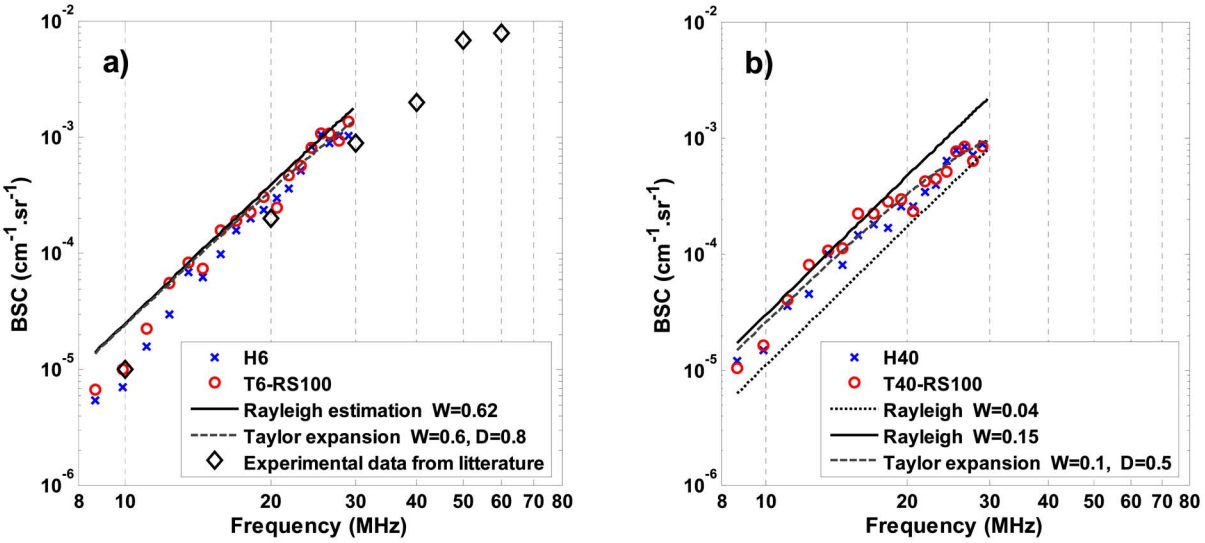

FIG. 1. (Color online) (a) Backscatter coefficient for H6 blood gently stirred in a beaker and T6 blood sheared at 100 s^{-1} in the Couette flow apparatus. The theoretical Rayleigh prediction [Eq. (1)], the second-order Taylor model with $W=0.6$ and $D=0.8$ [Eq. (10)], and H6 experimental data obtained by using nonfocused transducers (Refs. 15 and 16) are also plotted. (b) Backscatter coefficient for H40 blood sheared at 50 s^{-1} and T40 blood sheared at 100 s^{-1} in the Couette flow apparatus. The theoretical Rayleigh prediction with $W=0.04$ and $W=0.15$, and the second-order Taylor model with $W=0.1$ and $D=0.5$ are also plotted (see Table IV). Standard deviations are not shown for clarity.

submerged in degassed water and positioned in the focal plane of each transducer to provide normalization data. A window of 1024 points in each line was selected in the focal zone of the transducer and Fourier transformed; the amplitude was squared to get the power spectrum P of the backscattered signal. These data were then averaged over 100 acquisitions to provide $\overline{P_{H6B}}$ and $\overline{P_{plane}}$, where subscripts B and *plane* mean "beaker" and "planar reflector," respectively. The absolute backscatter BSC_{H6} of Rayleigh diffusers was measured by the substitution method with attenuation compensations, as suggested in[35]

$$BSC_{H6} = \frac{\overline{P_{H6B}(f,F)}}{\overline{P_{plane}(f,F)}} \frac{R_p^2 k^2 r^2}{8\pi d\left[1+\left(\frac{kr^2}{4F}\right)^2\right]} e^{(4\alpha_{H6}d)}, \qquad (11)$$

where R_p, k, r, d, F, and α_{H6} are, respectively, the reflection coefficient of the planar reflector (assumed to 1), the wave vector, the transducer radius, the inspected depth, the transducer focal length, and the H6 attenuation coefficient. This equation is valid in the focal zone of focused transducers for Rayleigh scatterers.[35] Such is the case for nonaggregated RBCs in our setup in the frequency range 9–30 MHz.[15] Since this step was not performed with nonfocused transducers, the results for BSC_{H6} are presented in Fig. 1(a) for validation.

Following the beaker and plane reflector measurements, each transducer was then successively placed in the Couette apparatus with its focal plane matching the center of the 2 mm gap between both concentric cylinders filled with blood. An agar gel was used to fill the hole that was made to position the transducer within the static cylinder; the solidified gel was cut to match the curvature of the cylinder in order to minimize any flow disturbance. The nonaggregating H6 sample was filled and gently sheared at 50 s^{-1} while acquiring 100 rf lines for each transducer. The shear rate was precisely controlled by the rotation speed of the moving Couette cylinder. The H6 data provided $\overline{P_{H6}}$ for the modified substitution method described in Eq. (12). Following these measures, the H6 sample was removed and the Couette apparatus was washed with saline. H40 was then introduced and rotated at the same shear rate of 50 s^{-1} in the Couette system. BSC_{H40} was computed also using Eq. (12) (with $\overline{P_{blood}}=\overline{P_{H40}}$) to provide comparison data for nonaggregating conditions at 40% hematocrit. Then, T6 and T40 whole blood samples were successively introduced in the Couette apparatus. For each aggregation kinetic experiment, the blood was first sheared at 100 s^{-1} for 2 min to disrupt RBC rouleaux. The shear rate was then changed to residual values of 0, 2, 10, and 30 s^{-1} for 3 min. During each experiment, 20 rf lines were acquired every 2 s for 190 s, starting 10 s before the application of the residual shear. At each time instant, a power spectrum was averaged over 20 rf lines to obtain $\overline{P_{blood}}$ in Eq. (12). The BSC of H6, H40, T6, and T40 samples, sheared in Couette flow, was computed as:

$$BSC_{blood} = BSC_{H6} \times \frac{\overline{P_{blood}}}{\overline{P_{H6}}} \times e^{4d(\alpha_{blood}-\alpha_{H6})}, \qquad (12)$$

where BSC_{H6} is given by Eq. (11) and α_{blood} is the attenuation coefficient of the investigated samples. Values of $\alpha_{H6} \approx \alpha_{T6} = 0.03$ dB/cm/MHz,[15] and $\alpha_{H40} \approx \alpha_{T40} = 0.22$ dB/cm/MHz[36,37] were selected for all shear rates.

Finally, since suspended RBCs are Rayleigh scatterers in the range of frequencies considered here,[15,16] theoretical values of BSC_{H6} and BSC_{H40} were also computed using Eqs. (1), (2), and (4). This second approach was used to confirm the experimental Couette flow measures of BSC. They are identified as "Rayleigh estimations" in Fig. 1. Using the H6 sample as a reference in the Couette rather than the beaker ensured that the focused beams were rigorously identical for

both spectra in the modified substitution method, as well as providing automatic attenuation compensation for the agar gel.

C. Microscopy analysis of RBC aggregates and segmentation

Aggregation kinetics of whole blood at 6% hematocrit (T6 sample) under static conditions were also quantified using an optical method. Blood was shaken using a pipette by cyclic aspiration and a drop was deposited on a glass lamella. It was covered by a micro lamella for visualization. Images were taken at an optical magnification of 40× (1 pixel $=0.6\times0.6$ μm) at intervals of 15 s during 3 min. This procedure was repeated three times with the same blood sample. A H6 nonaggregating suspension was also imaged for comparison. Grayscale images were processed offline to determine the size of each aggregate. The same algorithm was used on all images. First, a segmentation threshold was determined using images normalized in intensity between [0, 1]. The threshold minimized the intraclass variance of the black and white pixels by using the Otsu method (MATLAB function "Graythresh," version 7.0.1.24704, Natick, MA). From the binary images obtained by thresholding, all elements smaller than 7 pixels in diameter were eliminated since they were smaller than a single RBC (a typical single RBC had a diameter of 12 pixels). The size of each cluster of aggregates was normalized by a 12-pixel-diameter circular prototype to obtain the number of RBCs per aggregate. Following this preprocessing, the histogram of the number of RBCs per aggregate was traced and fitted to an exponential distribution of mean b, the mean number of RBCs per aggregate. Assuming isotropic 2D circular aggregates, as a first approximation, the surface occupied by b RBCs is given by $\pi(D_{\mathrm{OPT}}/2)^2$. An optical equivalent of parameter D, given after Eq. (10), was thus given by

$$D_{\mathrm{OPT}} = \sqrt{\frac{4}{\pi}b}. \tag{13}$$

IV. RESULTS

A. Ultrasonic characterization of RBC suspensions

Figure 1(a) shows BSC obtained with the three transducers on H6, the 6% hematocrit RBC suspension reference medium [Eq. (11)]. The BSC on T6 computed with Eq. (12) at 100 s^{-1} (T6-RS100, where RS means "residual shear") is also presented. The fitted Taylor model expansion [Eq. (10)] and the theoretical Rayleigh estimation [Eq. (1)] are also represented, along with experimental results from Refs. 15 and 16. Figure 1(b) shows BSC obtained on H40, the 40% hematocrit RBC suspension, the theoretical Rayleigh BSC with $W=0.04$ and $W=0.15$ [Eq. (4)] and the Taylor model. Values of W obtained with the Taylor model for suspended nonaggregating RBCs at 6% and 40% hematocrits are very close to the theoretical Perkus–Yevick predictions (see Table IV). In addition, the estimated value of $D=0.78\pm0.09$ for H6 is fairly close to the expected result of 1 RBC/aggregate, whereas the size estimation appears underestimated for H40 ($D=0.5\pm0.1$).

TABLE IV. Experimental and theoretical values of W and D for disaggregated RBCs suspended in an isotonic saline solution at 6% and 40% hematocrits. $W_{\mathrm{PY}s}$ and $W_{\mathrm{PY}c}$ were calculated using Eqs. (3) and (4).

	H6		H40	
	W	D	W	D
Experimental values	0.60±0.03	0.78±0.09	0.10±0.01	0.5±0.1
Theoretical $W_{\mathrm{PY}s}$	0.62	⋯	0.04	⋯
Theoretical $W_{\mathrm{PY}c}$	0.78	⋯	0.15	⋯
Theoretical D	⋯	1	⋯	1

B. Kinetics of RBC aggregation

Figure 2 presents the mean BSC over the respective transducers' bandwidth (see Table III) during the kinetics of rouleaux formation for (a) T6 and (b) T40 blood samples. At both studied hematocrits, the rouleaux formation kinetic profiles had similar shapes. For instance, at all frequencies, BSC first had a low value, when blood was sheared at 100 s^{-1}, which corresponds to the disaggregated state. BSC then gradually increased and stabilized at different levels depending on the applied residual shear rates and on the US frequency. The highest BSC levels were achieved at a residual shear rate of 2 s^{-1} for all experiments (RS2 curves). As expected, higher shearing (RS10 and RS30) partially disrupted RBC aggregates and smaller BSC were thus obtained. Under static conditions (RS0) and for all transducers, the BSC reached an intermediate level near that of RS10. For T40, faster kinetics were observed in the first few seconds at increasing frequencies.

Figure 3 shows the evolution of parameters W and D during the process of aggregate formation. As observed, W and D increased as a function of time for residual shear rates promoting RBC aggregation. The comparison of results at both hematocrits suggests that aggregates formed at 40% hematocrit are smaller in size than those obtained at 6% hematocrit, at each respective residual shear rate. Mean values at the plateau of the kinetic curves for all applied shear rates are summarized in Table V.

C. Frequency dependence of the BSC

Figure 4 shows BSC as a function of frequency for different residual shear rates and at the plateau of the kinetics of aggregation (temporal means between $t=170$ s and $t=180$ s). Standard deviations are not shown for clarity. It can be observed that BSC increases with the level of aggregation promoted by different residual shears. The BSC is Rayleigh at low frequencies and high shear rates, and becomes non-Rayleigh (drop in SS) with decreasing RS. Also represented in Fig. 4 are fitted curves based on the Taylor model. Respective values of W and D were reported earlier in Table V.

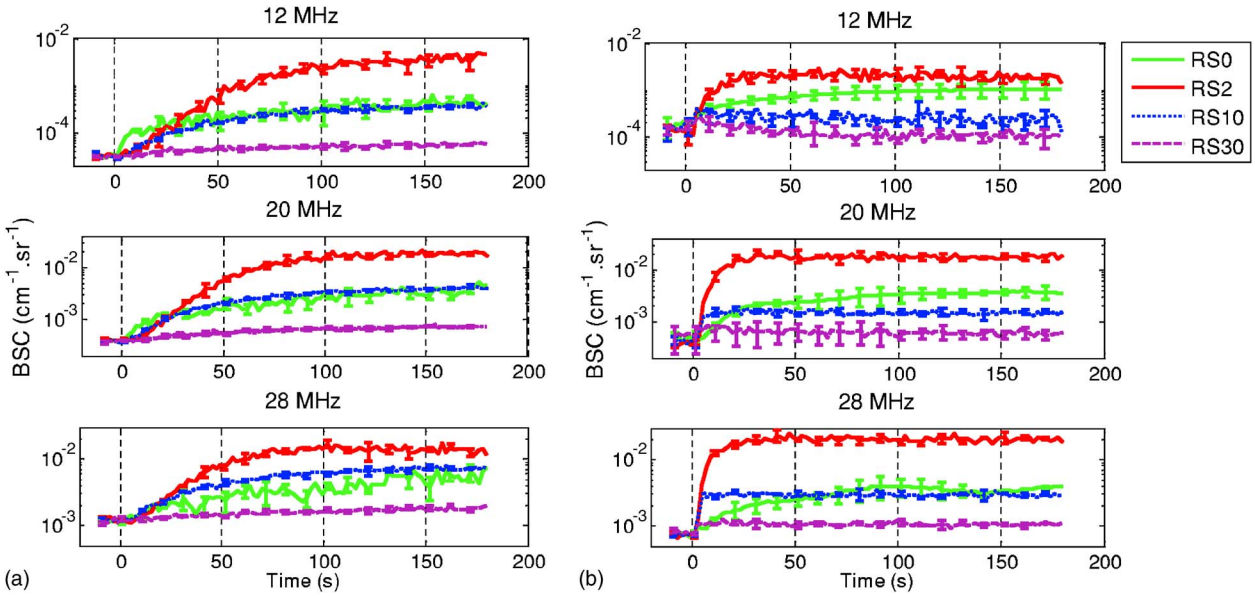

FIG. 2. (Color online) BSC during the kinetics of rouleaux formation for (a) T6 and (b) T40 blood at different residual shear rates of 0, 2, 10, and 30 s^{-1}. A high shear rate of 100 s^{-1} was first applied during the first 10 s (before $t=0$ s). BSC is taken as the mean value over the transducer bandwidth (see Table III). Results are expressed as means ±1 s.d. over three experiments.

D. Comparison of US and optical methods

The US data obtained under static conditions (RS0) are compared in this section with microscopic images acquired at the same hematocrit of 6%. Images were taken with a time resolution of 15 s during 3 min. The first row of Fig. 5 shows typical microscopic images during the aggregation kinetics promoted by Brownian motion. The actual treated images were bigger, only the central 300×400 pixels of the whole 960×1280 pixels are shown in Fig. 5. Binary thresholded images are presented in the second row. Segmented objects are given in the third row. Histograms of the number of RBCs per aggregate, arbitrarily partitioned in 15 logarithmically spaced bins, are displayed in Fig. 6. Each distribution was fitted to an exponential function defined by $P(x)=(1/b)e^{(-x/b)}$, where $b=\text{mean}(x)$ and x is the number of RBCs per aggregate. Parameter b is thus an estimation of the mean number of RBCs per 2D aggregate. D_{OPT} was computed using Eq. (13). Optical and acoustical estimations of D are compared in Table VI. Both methods show an increase of the aggregate size with time under static condition. The linear regression of D_{OPT} with $D_{(\text{US})}$ (see Fig. 7) resulted in an index of correlation $r^2=0.76$, reflecting that both methods followed the dimension of aggregates over time. In Fig. 7, the optical method generally predicted lower values of D.

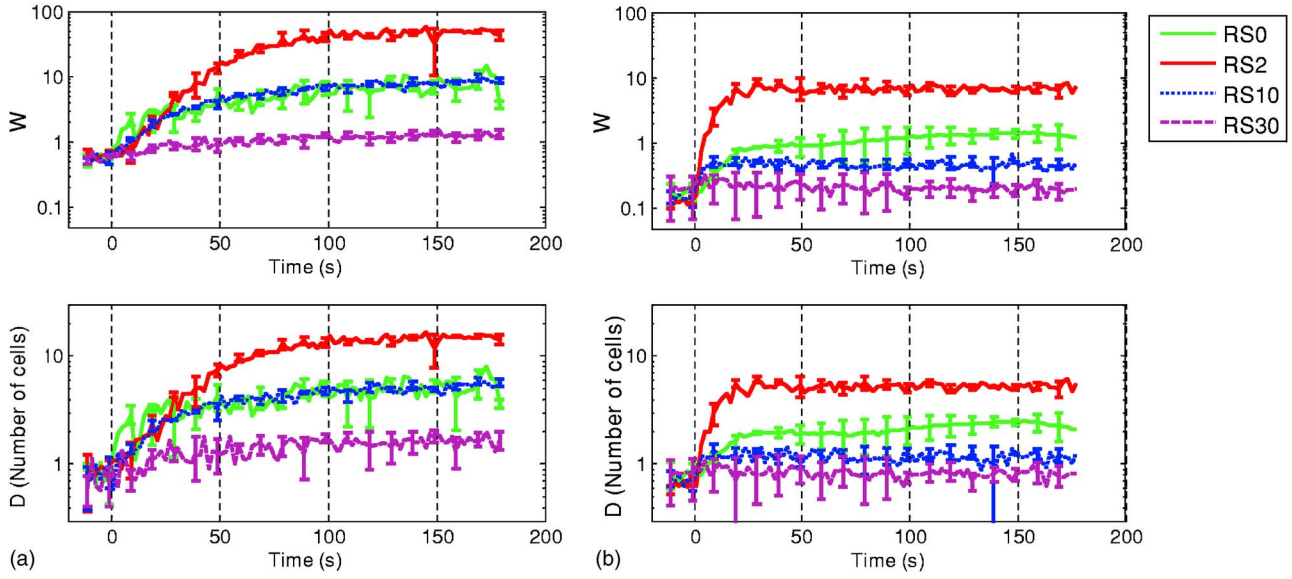

FIG. 3. (Color online) Time variations of fitted parameters W and D during the kinetics of RBC aggregation for experiments with (a) T6 blood and (b) T40 blood at different residual shear rates (RS=0, 2, 10, and 30 s^{-1}). A high shear of 100 s^{-1} was applied during the first 10 s of each acquisition. Results are expressed as means ±1 s.d. over three experiments.

TABLE V. T6 and T40 blood fitting parameters W and D at different residual shear rates (averaged values were computed between $t=170$ and 180 s). RS100 data were averaged between $t=0$ and 10 s. Results are expressed as means ±1 s.d. over three experiments.

Residual shear rate	T6		T40	
	W	D	W	D
RS0	6.8±2.4	4.9±1.4	1.4±0.1	2.4±0.1
RS2	48.9±5.7	15.0±1.0	6.8±1.1	5.3±0.6
RS10	8.4±0.7	5.3±0.4	0.5±0.1	1.1±0.1
RS30	1.3±0.2	1.6±0.3	0.2±0.1	0.7±0.1
RS100	0.60±0.09	0.87±0.27	0.2±0.03	0.8±0.1

V. DISCUSSION

A. On the quality of the data normalization

One concern when pursuing UTC is the quality and reliability of the normalization algorithm. A recent interlaboratory study[38] suggested that improvements in data normalization needed to be pursued, especially for BSC intensity measurements. However, that study also suggested that measurements of backscatter frequency dependent parameters, such as the spectral slope, were more consistent. We therefore tried, in the current study, to take advantage of BSC frequency-dependent information, while emphasizing the validation of the normalization procedure to achieve proper UTC.

First, we used three different transducers to obtain frequency-dependent backscatter measurements. The continuity in frequency can be appreciated in Figs. 1 and 4. Second, values of W obtained with our model for suspended nonaggregating RBCs at 6% and 40% hematocrits are very close to the theoretical Perkus–Yevick predictions. The estimated value of $D=0.78\pm0.09$ for H6 is also fairly close to the expected number of 1 RBC / aggregate, whereas the size estimation seems slightly underestimated for H40 ($D=0.5\pm0.1$, see Table IV). Lastly, as another validation step, one can note that the increases in BSC reported in this study as a function of the level of aggregation are comparable with published data from the literature. For instance, Yuan and Shung[19] reported aggregating pig blood backscattered power as a function of frequency at mean shear rates of 2, 10, and 22 s^{-1} using five unfocused transducers from 3.5 to 12.5 MHz. Hematocrits of 4.5%, 25%, and 45% were investigated in that study. The limitation of the Rayleigh scattering theory could be clearly observed as the spectral slope decreased for strongly aggregating RBCs at 10 MHz and higher, as can be noted with our data (Fig. 4). Our low hematocrit data [Fig. 4(a)] are also in agreement with those shown in Fig. 4 of Ref. 19. In that same study, an increase of 11.5 dB at 12.5 MHz was reported when the shear rate was decreased from 22 to 2 s^{-1} at 45% hematocrit. Our data [T40-RS2—Fig. 2(b)] suggests an increase of 12 dB from 30 to 2 s^{-1} at 12 MHz. In addition, a 13 dB increase at 30 MHz was measured between low and high shearing conditions for whole blood at physiological hematocrits in Refs. 24 and 23. Our data [T40-RS2—Fig. 2(b)] at 28 MHz shows a 14 dB increase with shear rate variations from 100 to 2 s^{-1}. It must be noted, nevertheless, that the former results were obtained on human blood rather than porcine blood. Other experimental studies have also found similar relative increases of the BSC with aggregation.[18,20,21] All these results tend to demonstrate the validity of Eq. (11) (normalization with BSC_{H6}) and of Eq. (12) that were used to obtain BSC_{T6}, BSC_{H40}, and BSC_{T40}.

B. BSC rate of increase during RBC aggregation kinetics

As observed in Fig. 2, the BSC increase in the first few seconds following flow reduction was faster as the frequency was increased; this is especially evident for a hematocrit of 40% and for residual shear rates promoting the largest aggregates. These results confirm previous observations at 40% hematocrit[22] where the rate of increase of the backscattered power as a function of time following flow stoppage was significantly faster at 58 and 36 MHz than at 10 MHz. It was postulated in that study that increasing the ultrasound frequency improved the sensitivity of the method to rapid changes in RBC aggregate sizes. When comparing in Fig. 2 results at 6% and 40% hematocrits, the more rapid increase of BSC at the highest hematocrit is not surprising if one considers that the probability of two RBCs to be in proximity is higher at 40% hematocrit.

C. Frequency-dependent data and second-order Taylor model

The SFSE can be seen as an implementation of form factors used in other tissue characterization fields,[39] adapted to the problem of RBC aggregation. In that sense, it takes into consideration the structure of the tissue rather than the shape of a single scatterer. $S(-2k)=W-4\ R_g^2k^2$ is a decreasing function of k from W to minus infinity.

The parallel is straightforward when illustrated with scarce scatterer concentration: in this case, W is equal to 1 and using $R_g=\sqrt{\frac{3}{5}}R$, then $S(-2k)=1-\frac{12}{5}R^2k^2$. With nonaggregated RBCs and for $f<30$ MHz ($ka<0.33$), $S(-2k)$ behaves similarly to the spherical Gaussian and to the exponential form factor, as shown in Fig. 8 (the notation R is used in this study but the notation a_{eff} is often found in the literature). The structure factor is a decreasing function in ka that translates a variation in scatterer organization but that can have a low frequency limit W different from unity. As Gaussian, fluid sphere, or spherical shell form factors describe the amplitude of the backscattered intensity due to a single scatterer as a function of the frequency, the structure factor describes the effect of aggregation on the backscattered intensity of increasingly organized weak scatterers. The main advantage is that the SFSE can be applied to dense media where the scatterers' positions are partially correlated. If scatterers in the tissue are independently positioned, $W=1$ and the SFSE is very similar to a form factor.

One might wonder why we limited our model to a second-order Taylor expansion in Eq. (10). If it is mathematically true that a higher polynomial order would provide a better fitting with the experimental data, we found that the physical pertinence of the model was lost when a higher

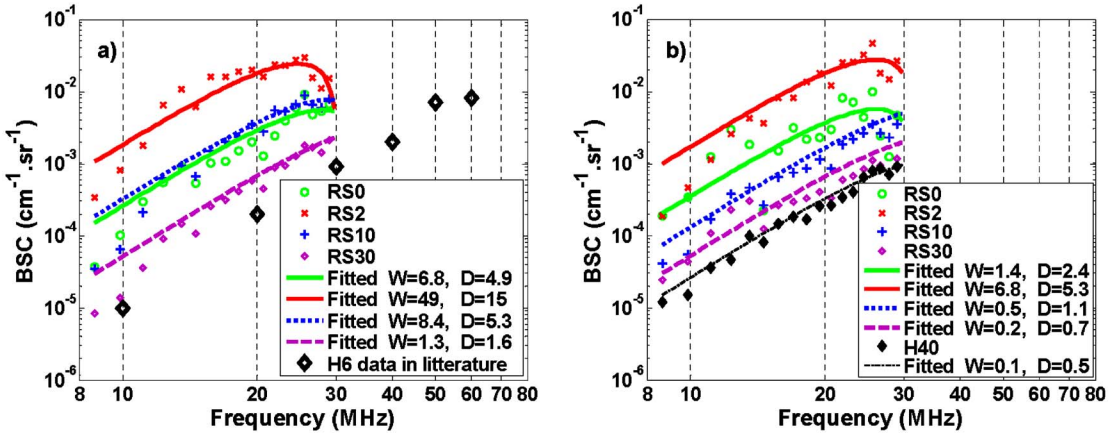

FIG. 4. (Color online) Frequency dependencies of (a) T6 and (b) T40 blood samples sheared at different residual shear rates (RS=0, 2, 10, and 30 s^{-1}), and corresponding fitted models. H6 experimental data taken from Refs. 15 and 16 are also displayed. The standard deviations are not shown for clarity.

order was used. For instance, the second-order model allowed the estimation of W and D, which have a physical meaning.

Also, one might question the physical meaning of $W>1$. In fact, Eqs. (3) and (4) are function of H and are strictly limited to $0<W\leqslant 1$. It is important to emphasize that the above equations were derived for nonaggregating particles. Moreover, our results for nonaggregated RBCs were consistent with these equations. As mentioned earlier, the packing factor W can be generalized for aggregating particles as the low frequency limit of the structure factor. This concept has been used earlier in the field of colloidal suspensions. The Baxter sticky hard sphere model was used to describe the effect of aggregation within the Perkus–Yevick approximation of the structure factor and its low frequency limit W.[40] The adhesive sphere model predicts values of W that decrease from 1 to 0 with increasing hematocrits for low adhesion energy, but presents values of $W>1$ when the adhesion energy is increased. Values of W up to 50 were reported at a volumic fraction of 12%. The structure factor at a frequency of 0 Hz [i.e., $S(0)=W$] is thermodynamically described in this model as $W=mKT\xi_T$ with K being the Boltzmann's constant, T the absolute temperature, and ξ_T the isothermal compressibility, as in Twersky's work.[30] It is also interesting to remark that an increase of W with aggregation is also consistent with an increase in variability of the number of scatterers per elemental scattering voxel, as suggested in Ref. 41.

D. Validation

There is no known way for the authors to experimentally characterize the real size of 3D RBC aggregates at a physiological hematocrit and hence to validate the dimensions reported here. For instance, microscopic observations can only be done with diluted blood; this is why we limited the optical validation to a hematocrit of 6%. Although the correlation between the US and optical methods was good ($r^2=0.76$), it is clear that the comparison has limitations. We can consider the 2D nature of the wet mounts for microscopy versus the 3D structure of real aggregates sensed with US, the isotropic nature of the estimators versus the anisotropic shape of real rouleaux networks, and the limitation of the optical method that only considered a static condition. However, some quantitative information could be deduced with our second-order model. The estimated parameters W and D were modulated in a predictable manner by the applied residual shear rate: Higher shear rates produced smaller values of those measures due to the reversible disruption of RBC clusters. The fact that aggregates were smaller under static conditions is

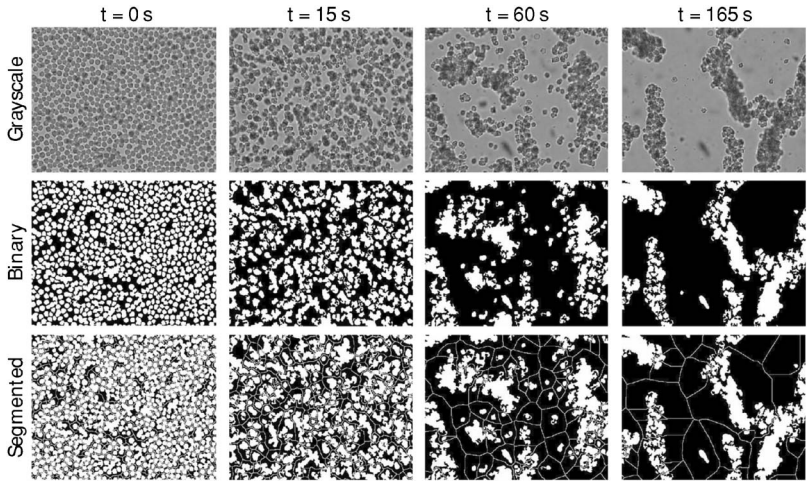

FIG. 5. Columns represent typical microscopic images and image processing at a particular time during the kinetics of aggregation of a T6 sample. Rows represent grayscale images, binary images, and segmented images. Actual processed images (960×1280 pixels) were bigger than those represented here (300×400 pixels). Resolution is 1 pixel=0.6 μm×0.6 μm.

TABLE VI. Estimations of D with the optical and ultrasonic methods. Microscopic images were acquired with a time resolution of 15 s. A time resolution of 30 s was used here to reduce the size of the table. US data taken from Fig. 3 (RS0, H=6%) at corresponding times were used for comparison.

Time (s)	0	30	60	90	120	150	180
D_{OPT}	1.5±0.3	2.4±0.3	3.1±0.5	3.5±0.4	4.2±0.2	4.5±0.1	4.7±0.1
D_{US}	0.8±0.1	3.9±0.1	3.8±0.6	5.3±0.4	4.9±1.0	4.8±1.0	6.2±1.1

not surprising. Others have reported that a minimal level of shear is necessary to promote aggregation, as it increases RBC interactions.[42–44] Further increasing the shear rate results in the breaking of rouleaux. Furthermore, our model showed smaller values of W and D at 40% vs 6% hematocrit. This observation was made earlier in Ref. 45, where the radius of gyration of concentrated cluster suspensions was studied. Stronger aggregate interpenetrations at high hematocrit were hypothesized in that study to explain this observation. Another group reported size estimations from computerized image analysis of RBC aggregates in a small flow chamber.[46] With a diluted 10% hematocrit blood, they measured aggregates of about 6–12 RBCs/aggregate at stasis ($\sim$0 dyn/cm^2) and of about 24–48 RBCs/aggregate at a low shear stress of $\sim$0.1 dyn/cm^2 (corresponding to a shear rate of 10 s^{-1} considering plasma as a Newtonian fluid of viscosity=1 cP).

E. Respective effect of W and D on the second-order Taylor model, relation $(D)^2 \rightarrow W$

To help interpret the acoustical meaning of W and D and the relation between these two physical parameters, we first present in Fig. 9 for T6-RS100 the respective effect of varying W and D on the BSC; we arbitrarily selected a shear rate of 100 s^{-1}, the same interpretation applies to the other shear rates. An increase in W has the effect of increasing the amplitude of the BSC at all frequencies. In terms of standard UTC measures, it can be seen as an analogue to the mean BSC.[47] Increasing D has an effect on the frequency dependence and it thus modulates the spectral slope SS.

Another interesting aspect of parameters W and D, apart from their physical interpretability ("packing factor" and "normalized mean aggregate size"), is the fact that they are not independent from one another. In Fig. 10 are plotted W as a function of $(D)^2$ for all blood samples during the entire kinetics of aggregation for 6% and 40% hematocrits and for all applied shear rates. It can be clearly observed that a quadratic relation exists between W and D. Although this observation could have led us to eliminate one parameter in our data reduction model, we chose not to, as D brings a physical dimension and W is a parameter largely studied in UBC. The fact that the 40% hematocrit scales in the same way as the 6% hematocrit brings further confidence in the second-order approximation model. The relation between both parameters should be further investigated in future studies.

F. Guinier plot

One convenient way to determine the higher frequency limit of our second-order approximation is to use the Guinier plot. This plot is frequently used in x-ray, neutron, and light scattering characterization. It consists in plotting $k^2 \rightarrow \log S(-2k)$. Since we are dealing with a second-order model, the quadratic approximation is valid when the slope is linear in the so-called Guinier region. In Fig. 11 are plotted Guinier results for T6 and T40 blood samples at a residual shear of 2 s^{-1}. The frequency correspondence of the abscissa is indicated by arrows in Fig. 11. Very interesting information can be deduced from Fig. 11. First, the T6-RS2 Guinier plot diverges from a linear slope at frequencies higher than

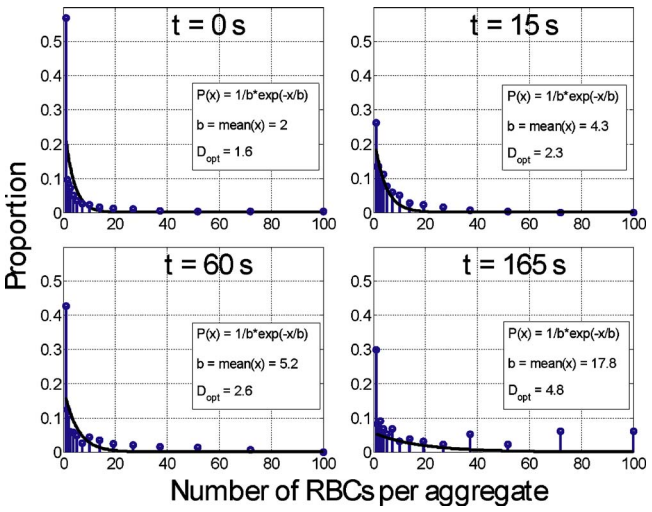

FIG. 6. (Color online) Histograms of the aggregate dimension in number of cells at times 0, 15, 60, and 165 s. Cell count was arbitrarily separated in 15 logarithmically spaced bins to allow better resolution for small sizes. The distributions were fitted by an exponential function of mean b defined by $P(x)=(1/b)\exp^{(-x/b)}$. D_{opt} was determined using Eq. (13).

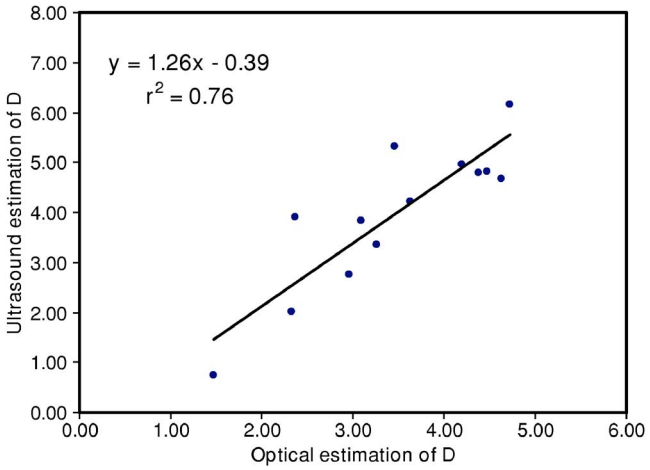

FIG. 7. (Color online) Comparison of D estimated with the optical and US methods. Each point is the mean over three experiments at a particular time during the kinetics of aggregation.

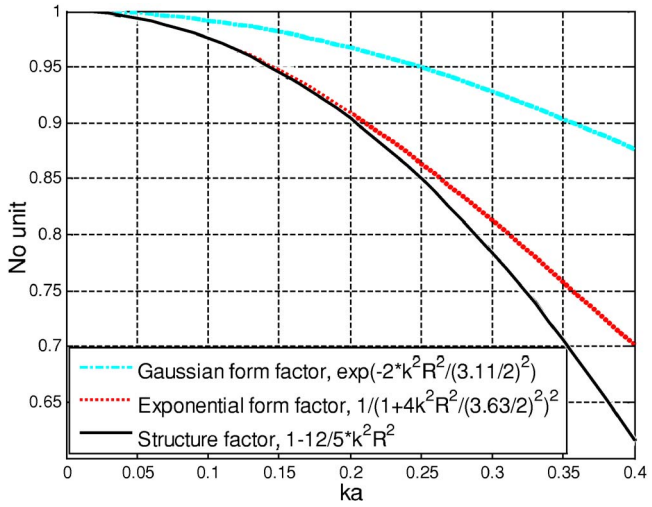

FIG. 8. (Color online) Spherical Gaussian form factor, exponential form factor, and the second-order Taylor expansion of the structure factor as a function of ka, for diluted scatterers ($W=1$). R, the effective radius of the scatterer, is often denoted as a_{eff} in the literature.

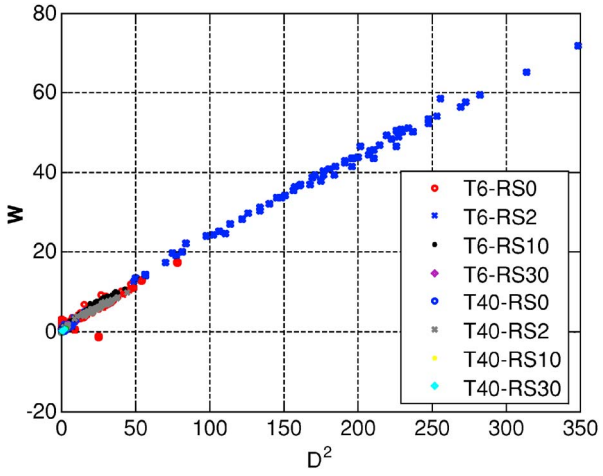

FIG. 10. (Color online) Quadratic relationship between D and W for all shear rates at both 6% and 40% whole blood hematocrits. The high frequency limit was fixed at 30 MHz.

33 MHz. This observation signifies that the second-order approximation is no longer valid for big aggregates at frequencies above 33 MHz. For this reason, we limited our second-order approximation to 30 MHz (see Sec. III). The same cannot be said about the Guinier plot of T40-RS2 that was still linear through 45 MHz. This observation also supports the preceding observation that aggregates formed at 40% hematocrit were smaller that those at 6% hematocrit, for any given residual shear rate.

VI. CONCLUSION

Experimental and theoretical results on BSC variations during the kinetics of RBC aggregation determined by modulating the shear rate in a Couette flow apparatus were presented. Different samples of whole blood and RBC suspensions at 6% and 40% hematocrits were prepared and quantitatively characterized at room temperature using three focused wideband transducers covering the bandwidth from 9 to 30 MHz. A second-order Taylor approximation of the structure factor, the SFSE, was proposed to achieve data reduction of the BSC measurements, to extract two physical parameters, namely the packing factor (W) and the mean normalized dimension of isotropic aggregates (D). The D parameter was validated by an optical imaging method at 6% hematocrit under static conditions. The SFSE presents an interesting framework for ultrasonic characterization of partially correlated tissues, such as aggregating blood. For instance, it more closely mimics the frequency dependence of BSC and it is physically interpretable in a non-frequency-dependent manner.

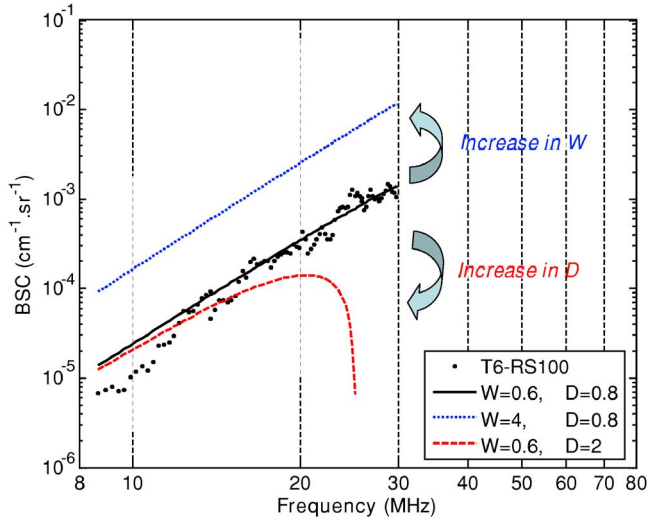

FIG. 9. (Color online) Effect of increasing W and D on the BSC in the second-order model.

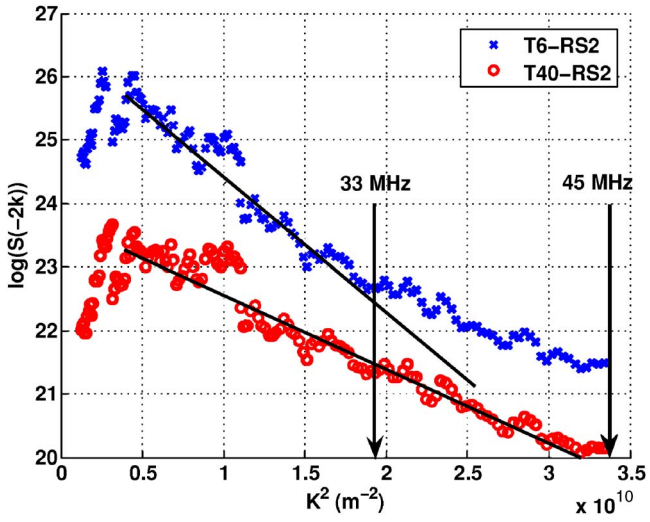

FIG. 11. (Color online) Guinier plots extended to 45 MHz for T6-RS2 and T40-RS2. The linear slope transition indicates the limit of the Guinier domain.

ACKNOWLEDGMENTS

This work was supported by Grant No. MOP-36467 from the Canadian Institutes of Health Research. The salary of F.T.H.Y. is partially supported by a Ph.D. studentship from the Natural Sciences and Engineering Research Council of Canada, and G.C. is recipient of the National Scientist Award from the "Fonds de la Recherche en Santé du Québec." We are also thankful to G. Leblond for his help in the segmentation of the microscopic images, and "Les Viandes ULTRA Meats Inc.," Saint-Esprit, Québec, Canada for blood supply.

[1]E. J. Feleppa, C. R. Porter, J. Ketterling, P. Lee, S. Dasgupta, S. Urban, and A. Kalisz, "Recent developments in tissue-type imaging (TTI) for planning and monitoring treatment of prostate cancer," Ultrason. Imaging **26**, 163–172 (2004).

[2]M. C. Kolios, G. J. Czarnota, M. Lee, J. W. Hunt, and M. D. Sherar, "Ultrasonic spectral parameter characterization of apoptosis," Ultrasound Med. Biol. **28**, 589–597 (2002).

[3]A. S. Tunis, G. J. Czarnota, A. Giles, M. D. Sherar, J. W. Hunt, and M. C. Kolios, "Monitoring structural changes in cells with high-frequency ultrasound signal statistics," Ultrasound Med. Biol. **31**, 1041–1049 (2005).

[4]F. Padilla, L. Akrout, S. Kolta, C. Latremouille, C. Roux, and P. Laugier, "In vitro ultrasound measurement at the human femur," Calcif. Tissue Int. **75**, 421–430 (2004).

[5]M. L. Oelze, W. D. O'Brien, Jr., J. P. Blue, and J. F. Zachary, "Differentiation and characterization of rat mammary fibroadenomas and 4T1 mouse carcinomas using quantitative ultrasound imaging," IEEE Trans. Med. Imaging **23**, 764–771 (2004).

[6]J. Mamou, M. L. Oelze, W. D. O'Brien, Jr., and J. F. Zachary, "Identifying ultrasonic scattering sites from three-dimensional impedance maps," J. Acoust. Soc. Am. **117**, 413–423 (2005).

[7]V. Giglio, V. Pasceri, L. Messano, F. Mangiola, L. Pasquini, A. Dello Russo, A. Damiani, M. Mirabella, G. Galluzzi, P. Tonali, and E. Ricci, "Ultrasound tissue characterization detects preclinical myocardial structural changes in children affected by Duchenne muscular dystrophy," J. Am. Coll. Cardiol. **42**, 309–316 (2003).

[8]S. Chien, "Biophysical behavior of red cells in suspensions," in *The Red Blood Cell*, edited by D. M. Surgenor (Academic, New York, 1975), Vol. II, Chap. 26, pp. 1031–1133.

[9]E. Alt, S. Banyai, M. Banyai, and R. Koppensteiner, "Blood rheology in deep venous thrombosis—Relation to persistent and transient risk factors," Thromb. Res. **107**, 101–107 (2002).

[10]A. J. Lee, P. I. Mowbray, G. D. O. Lowe, A. Rumley, F. G. R. Fowkes, and P. L. Allan, "Blood viscosity and elevated carotid imtima-media thickness in men and women. The Edinburgh artery study," Circulation **97**, 1467–1473 (1998).

[11]C. Le Devehat, M. Vimeux, and T. Khodabandehlou, "Blood rheology in patients with diabetes mellitus," Clin. Hemorheol Microcirc **30**, 297–300 (2004).

[12]K. K. Shung, "On the ultrasound scattering from blood as a function of hematocrit," IEEE Trans. Sonics Ultrason. **SU-29**, 327–331 (1982).

[13]F. L. Lizzi, M. Ostromogilsky, E. J. Feleppa, M. Rorke, and M. M. Yaremko, "Relationship of ultrasonic spectral parameters to features of tissue microstructure," Ultrasonics **33**, 319–329 (1986).

[14]M. F. Insana, R. F. Wagner, D. G. Brown, and T. J. Hall, "Describing small-scale structure in random media using pulse-echo ultrasound," J. Acoust. Soc. Am. **87**, 179–192 (1990).

[15]S. H. Wang and K. K. Shung, "An approach for measuring ultrasonic backscattering from biological tissues with focused transducers," IEEE Trans. Biomed. Eng. **44**, 549–554 (1997).

[16]S. Maruvada, K. K. Shung, and S. Wang, "High-frequency backscatterer and attenuation measurements of porcine erythrocyte suspensions between 30–90 MHz," Ultrasound Med. Biol. **28**, 1081–1088 (2002).

[17]K. K. Shung, R. A. Sigelmann, and J. M. Reid, "Scattering of ultrasound by blood," IEEE Trans. Biomed. Eng. **BME-23**, 460–467 (1976).

[18]G. Cloutier, Z. Qin, L. G. Durand, and B. G. Teh, "Power Doppler ultrasound evaluation of the shear rate and shear stress dependences of red blood cell aggregation," IEEE Trans. Biomed. Eng. **43**, 441–450 (1996).

[19]Y. W. Yuan and K. K. Shung, "Ultrasonic backscatter from flowing whole blood. II. Dependence on frequency and fibrinogen concentration," J. Acoust. Soc. Am. **84**, 1195–1200 (1988).

[20]V. Rouffiac, P. Péronneau, A. Hadengue, A. Barbet, P. Delouche, P. Dantan, N. Lassau, and J. Levenson, "A new ultrasound principle for characterizing erythrocyte aggregation—In vitro reproducibility and validation," Invest. Radiol. **37**, 413–420 (2002).

[21]F. Yu, D. Savery, A. Amararene, F. S. Foster, and G. Cloutier, "Attenuation compensated spectral slopes during the kinetics of rouleaux formation for porcine whole blood in couette flow at 10–70 MHz," IEEE UFFC Proceedings, 2004, pp. 842–845.

[22]G. Cloutier, M. Daronat, D. Savery, D. Garcia, L. G. Durand, and F. S. Foster, "Non-Gaussian statistics and temporal variations of the ultrasound signal backscattered by blood at frequencies between 10 and 58 MHz," J. Acoust. Soc. Am. **116**, 566–577 (2004).

[23]F. S. Foster, H. Obara, T. Bloomfield, L. K. Ryan, and G. R. Lockwood, "Ultrasound backscatter from blood in the 30 to 70 MHz frequency range," Proc.-IEEE Ultrason. Symp. 1599–1602 (1994).

[24]M. S. Van Der Heiden, M. G. M. De Kroon, N. Bom, and C. Borst, "Ultrasound backscatter at 30 MHz from human blood: Influence of rouleau size affected by blood modification and shear rate," Ultrasound Med. Biol. **21**, 817–826 (1995).

[25]I. Fontaine, M. Bertrand, and G. Cloutier, "A system-based approach to modeling the ultrasound signal backscattered by red blood cells," Biophys. J. **77**, 2387–2399 (1999).

[26]I. Fontaine, D. Savéry, and G. Cloutier, "Simulation of ultrasound backscattering by red cell aggregates: Effect of shear rate and anisotropy," Biophys. J. **82**, 1696–1710 (2002).

[27]I. Fontaine and G. Cloutier, "Modeling the frequency dependence (5–120 MHz) of ultrasound backscattering by red cell aggregates in shear flow at a normal hematocrit," J. Acoust. Soc. Am. **113**, 2893–2900 (2003).

[28]D. Savery and G. Cloutier, "Effect of red cell clustering and anisotropy on ultrasound blood backscatter: A Monte Carlo study," IEEE Trans. Ultrason. Ferroelectr. Freq. Control **52**, 94–103 (2005).

[29]L. Y. L. Mo and R. S. C. Cobbold, "Theoretical models of ultrasonic scattering in blood," in *Ultrasonic Scattering in Biological Tissues*, edited by K. K. Shung and G. A. Thieme (CRC Press, Boca Raton, FL, 1993) Chap. 5, pp. 125–170.

[30]V. Twersky, "Low-frequency scattering by correlated distributions of randomly oriented particles," J. Acoust. Soc. Am. **81**, 1609–1618 (1987).

[31]V. Twersky, "Transparency of pair-correlated, random distributions of small scatterers, with application to the cornea," J. Opt. Soc. Am. **65**, 524–530 (1975).

[32]B. G. Teh and G. Cloutier, "Modeling and analysis of ultrasound backscattering by spherical aggregates and rouleaux of red blood cells," IEEE Trans. Ultrason. Ferroelectr. Freq. Control **47**, 1025–1035 (2000).

[33]A. Guinier and J. Fournet, *Small Angle Scattering of X-Rays* (Wiley Interscience, New York, 1955).

[34]Y. W. Yuan and K. K. Shung, "The effect of focusing on ultrasonic backscatter measurements," Ultrason. Imaging **8**, 121–130 (1986).

[35]M. Ueda and Y. Ozawa, "Spectral analysis of echos for backscattering coefficient measurement," J. Acoust. Soc. Am. **77**, 38–47 (1985).

[36]J. F. Greenleaf, *Tissue Characterization with Ultrasound I*, 1st ed (CRC Press, Boca Raton, FL, 1986), Vol. 1.

[37]J. F. Greenleaf, *Tissue Characterization with Ultrasound II*, 1st ed. (CRC Press, Boca Raton, FL, 1986), Vol. 2.

[38]K. A. Wear, T. A. Stiles, G. R. Frank, E. L. Madsen, F. Cheng, E. J. Feleppa, C. S. Hall, B. S. Kim, P. Lee, W. D. O'Brien, Jr., M. L. Oelze, B. I. Raju, K. K. Shung, T. A. Wilson, and J. R. Yuan, "Interlaboratory comparison of ultrasonic backscatter coefficient measurements from 2 to 9 MHz," J. Ultrasound Med. **24**, 1235–1250 (2005).

[39]K. K. Shung and G. A. Thieme, *Ultrasonic Scattering in Biological Tissues*, edited by K. K. Shung and G. A. Thieme (CRC Press, Boca Raton, 1993).

[40]C. Regnaut and J. C. Ravey, "Application of the adhesive sphere model to the structure of colloidal suspensions," J. Chem. Phys. **91**, 1211–1221 (1989).

[41]L. Y. L. Mo and R. S. C. Cobbold, "A stochastic model of the backscattered Doppler ultrasound from blood," IEEE Trans. Biomed. Eng. **BME-33**, 20–27 (1986).

[42]H. Schmid-Schönbein, P. Gaehtgens, and H. Hirsch, "On the shear rate dependence of red cell aggregation in vitro," J. Clin. Invest. **47**, 1447–1454 (1968).

[43]R. E. N. Shehada, R. S. C. Cobbold, and L. Y. L. Mo, "Aggregation effects in whole blood: Influence of time and shear rate measured using ultrasound," Biorheology **31**, 115–135 (1994).

[44]Z. Qin, L. G. Durand, and G. Cloutier, "Kinetics of the 'black hole' phenomenon in ultrasound backscattering measurements with red blood cell aggregation," Ultrasound Med. Biol. **24**, 245–256 (1998).
[45]P. Snabre and P. Mills, "Rheology of weakly flocculated suspension of rigid particles," J. Phys. III **6**, 1811–1834 (1996).
[46]S. Chen, G. Barshtein, B. Gavish, Y. Mahler, and S. Yedgar, "Monitoring of red blod cell aggregability in a flow-chamber by computerized image analysis," Clin. Hemorheol. **14**, 497–508 (1994).
[47]F. L. Lizzi, M. Greenebaum, E. J. Feleppa, M. Elbaum, and D. J. Coleman, "Theoretical framework for spectrum analysis in ultrasonic tissue characterization," J. Acoust. Soc. Am. **73**, 1366–1373 (1983).
[48]Y. W. Yuan and K. K. Shung, "Ultrasonic backscatter from flowing whole blood. I: Dependence on shear rate and hematocrit," J. Acoust. Soc. Am. **84**, 52–58 (1988).